Physica E 117 (2020) 113851

Contents lists available at ScienceDirect

Physica E: Low-dimensional Systems and Nanostructures

journal homepage: http://www.elsevier.com/locate/physe

Formation of composite nanostructures with an effective hydrazine sensor and their chemical approach

Rizwan Wahab [a,*], Naushad Ahmad [b], Manawwer Alam [b], Javed Ahmad [a]

[a] Zoology Department, College of Science, King Saud University, Riyadh, 11451, Saudi Arabia
[b] Department of Chemistry, College of Science, King Saud University, P.O. Box 2455, Riyadh, 11451, Saudi Arabia

ARTICLE INFO

Keywords:
Nanocomposite
Hydrazine
Glassy carbon electrode (GCE)
Sensor

ABSTRACT

In this paper, the composite of nickel and cobalt was synthesized via nickel nitrate and cobalt nitrate hexahydrate as nickel cobalt oxide (NiCoO) processed via chemical solution approach. The chemicals such as the nickel nitrate hexahydrate, cobalt nitrate hexahydrate and sodium hydroxide were utilized to form a solution and it refluxed at ~90 °C for 60 min for formation of nanocomposite of NiCoO. Thereafter, the obtained composite of NiCoO was well characterized with the instruments such as X-ray diffraction pattern (XRD), scanning electron microscopy (SEM), transmission electron microscopy (TEM), fourier transform infrared (FT IR) and X-ray photoelectron spectroscopy (XPS) also with electrochemical data. The well crystalline formed nanoparticles have been employed as an electroactive material for high sensitive hydrazine sensor detection with glassy carbon electrode (GCE). The electro chemical characterization was analyzed with cyclic voltammetry (CV) data's at very low to high concentration (2 μL–2 mL/100 mL PBS), effect of scan rate was analyzed from 10 to 100 mVs^{-1} with NiCoO/GCE electrode. The proposed sensor and their stability are the promising features of the sensor.

1. Introduction

Hydrazine (NH_2) is a compound which extensively and especially employed in chemical, agriculture, and pharmaceutical industry. It is also used as an antioxidants, propellant, fuel, corrosion inhibitors, catalysts, emulsifier, plant growth regulator (insecticide, herbicide, and pesticides), pharmaceutical intermediates, plastic blowing agents, and photographic agents etc [1–5]. Regardless of their multi-worth applications, the exposure at minute quantity to ecosystem it causes dizziness, dermatitis, short-term blindness, and irritation of eyes, nose, and throat due to its toxic in nature [6,7]. Therefore, World Health Organization (WHO) and United States Environmental Protection Agency are classified as group B2 human carcinogens [8]. Because of its toxic nature limits application in many of advanced felids; therefore, it's an urgent need to develop simple, sensitive, and low-cost economic techniques and materials for the detection with cost effective ways. Earlier various methods have been developed such as colorimetric titration [9], chromatography [10,11], chemiluminescence [12], flow injection analysis [13] spectrophotometry [14], potentiometry, and so on [15] for the detection were employed, but many of these techniques involve tedious and time-consuming protocols. In contrast, the electrochemical sensing methods, which is very simple, low-cost fabrication process and high sensitivity, selectivity and reliability with rapid response [16–41]. The electrochemical sensing of hazardous chemicals including hydrazine by modification of working electrode with different types of materials such as carbon nanotubes [16], graphene oxides [17–20], composites [21], metals and its oxides (supported and unsupported) [22–24] have better advantages than conventional bare electrode. Towards this direction, Sun et al prepared a series of MgOx-Al_2O_3 composite oxides with diverse shaped crystal structures from the impregnation-calcination technique. To this composite, gold nanoparticles are highly selective and supportive catalysts for hydrogenation of acetylene, explored many possibilities for highly efficient heterogeneous catalyst [42]. The yolk-shell nanostructures with mixed metals/nanocomposite such as SnO_2/Au/Fe_2O_3 nanoboxes with a specific surface area was successfully prepared and used for the detection and development of a gas sensor. The prepared SnO_2/Au/Fe_2O_3 yolk-shell nanostructures displayed an outstanding response against triethylamine (TEA) gas at 240 °C [43]. With the recent advances in nanotechnology, nanoparticles (NPs) with various shapes has been drawn a considerable attention for the detection of environmentally toxic chemicals via electrochemical process because of their exceptional assets along with very high sensitivity of NPs [44].

* Corresponding author. College of Science, Department of Zoology, P.O. Box 2455, King Saud University, Riyadh, 11451, Saudi Arabia.
E-mail addresses: rwahab@ksu.edu.sa, rwahab05@gmail.com (R. Wahab).

https://doi.org/10.1016/j.physe.2019.113851
Received 23 April 2019; Received in revised form 28 October 2019; Accepted 22 November 2019
Available online 23 November 2019
1386-9477/

Among various nanostructured material, mixed or bimetallic metal oxides nanocomposites have been found extensive applications in electrochemical sensing due to their interesting electronic, optical, electrocatalytic properties [25–34]. Some of the nanomaterials (NMs) have been successfully employed for rapid electrochemical detection of hydrazine [27–34]. In electrochemical sensing research area, key factor is to improve the materials conductivity for better interface between electrode and electrolytes. Traditionally, metallic and non-metallic dopants or appropriate supported material will be introduced into the lattice of metal oxides [35–37]. Over various transition metals, nickel oxide (NiO) is commonly used as an electrochemical performance but it suffers from poor conductivity, which particularly restricts its many applications [38–41]. Therefore, in present, we have synthesized the nickel doped cobalt oxide (NiCoO) NPs via solution method in liquid medium at reduced refluxing temperature. The prepared NPs morphology was evaluated via SEM and TEM, whereas crystallinity and functional composition were examined via X-ray diffraction pattern and FTIR spectroscopy with the required instruments respectively. Further, the electrochemical sensing toward hydrazine was evaluated by cyclic voltammetry (CV), amperometry and electrochemical impedance spectroscopy (EIS) was evaluated.

2. Material and methods

2.1. Experimental

2.1.1. Synthesis of nickel cobalt (NiCoO) nanocomposite

The required reagents such as nickel nitrate hexahydrate (Ni $(NO_3)_2{\cdot}6H_2O$), cobalt nitrate (Co $(NO_3)_2{\cdot}6H_2O$), sodium hydroxide (NaOH) for the formation of nanocomposite were purchased from sigma–Aldrich chemical corporation, Riyadh Saudi Arabia and used as received. For the synthesis of nickel cobalt (NiCoO) nanocomposite, nickel nitrate hexahydrate ($Ni(NO_3)_2{\cdot}6H_2O$,0.3M), cobalt nitrate hexahydrate ($Co(NO_3)_2{\cdot}6H_2O$,0.3 M) were mixed in 100 mL of methanol (MeOH) solvent. To this mixture, sodium hydroxide (NaOH, 0.1 M) was added slowly for the formation of hydroxide molecules under constant stirring up to 30 min and the overall solution pH (pH meter, coleparmer, U.S.A) was measured which reached to 12.63. After the complete mixing of prepared solution, it was transferred to a refluxing pot (capacity 250 mL) fixed with condenser, refluxed at 90 °C for ~60 min. As per the observations, when the refluxing temperature upsurges, the color of the solution changes from bluish to black due to cobalt. After refluxing, the obtained precipitate was recovered in a glass beaker and washed several times with alcohol and acetone to eliminate the ionic impurities and thereafter dried in a glass pertidish at room temperature and to keep for further analysis.

2.1.2. Characterizations of synthesized nanocomposite

The prepared nanocomposites powder structural morphology was observed via SEM (Jeol, JE D-2200 series, Japan) at room temperature. For the SEM observation, the prepared powder was uniformly scattered on a carbon tape and coated with conducting layer of platinum (Pt) for 3–4 s. Then, the sample was fixed in a sample holder and analyzed at room temperature. Further the morphological investigation was again analyzed via TEM at room temperature. For this, powder sample was dissolved in an ethanol and prepared a suspension solution. To this suspensionsolution a copper grid was dipped for a sec and removed it from the solution. The copper grid was dried on hot plate with gentle heating and fixed it in a sample holder for further analysis. The crystallinity, phases, and size of the prepared black colored composite was analyzed via XRD (PANalytical XPert Pro, U.S.A.) with $Cu_{K\alpha}$ radiation ($\lambda = 1.54178$ Å) in range from 20 to 80° with 6°/min scanning speed. The functional properties of the prepared composite powder was examined by using Fourier transform infrared (FTIR; Perkin Elmer-FTIR Spectrum-100) in the range of 400–4000 cm^{-1}. The surface characteristic of the prepared nanocomposite was examined through X-ray photoelectron spectroscopy (XPS, AXIS-NOVA, Kratos Inc.) with $Al_{K\alpha}$ as a source of X-rays [45].

2.1.3. Hydrazine sensor based on nickel cobalt oxide nanocomposite (NiCoO)

The NiCoO nanocomposite was employed as an electron mediator/working electrode for to check and sense the N_2H_4 in chemical solution. To form this arrangement, the prepared NiCoO nanocomposite were coated on polished GCE electrode (active surface area = 0.071 cm^2). For coating, the slurry of NiCoO was made with butyl carbitol acetate (BCA) in a particular ratio (70:30%) respectively, and then the prepared slurry was coated on GCE electrode and dried at 60±5 °C for 6 h to get a uniform layer over entire electrode surface. The electrochemical measurements were carried out on Autolab Potentiostat/ galvanostat, PG STAT 204-FRA32 control with NOVA software (Metrohom Autolab B.V. Kanaalweg 29-G, 3526 KM Utrecht, Netherlands) in three electrode system [41]. The modified NiCoO/GCE electrode was used as working electrode, a Pt wire as a counter electrode and an Ag/AgCl (sat.KCl) was used as reference electrode. For all the measurements, 0.1 M phosphate buffer solution (PBS; pH 7.2) with hydrazine was used as an electrolyte solution. A wide conc., range of hydrazine from 2 μL to 10μL/100 mL PBS was opted to control the sensing characteristics with current response measured from −0.2 to +2.0 V. The sensitivity of fabricated nanocomposite based chemical sensor was estimated from the slope of the current vs concentration from the calibration plot divided by the value of active surface area of sensor/electrode. The amperometric current-time (i-t) curves were also measured at a potential of 0.5 V in stirring 0.1 M PBS solution. For the detection of real sample, 10 μL of hydrazine was added to 100 mL PBS solution.

3. Result and discussions

3.1. X-ray diffraction result of prepared nanocomposite powder

The XRD pattern depicts the size, phase and crystalline character of the processed powder from 20 to 80° with 6°/min scanning speed with 40 kV and 40 mA current at room temperature. The acquired data clearly demonstrates that almost all peaks and their positions (<223> (36.84), <330> (42.79), <167> (62.09), <68> (74.39) and <42> (78.30), are analogous and this can be accessible via powder diffraction data JCPDS 73-1704 including the lattice constant a = 9.387 (Fig. 1). From the obtained information the prepared composite exhibit a face centered cubic (FCC) system in their crystal geometry and it reveals that the powder is crystalline in nature and correspondents to phases of commercial powder of nickel and cobalt content of NiCoO nanocomposite. From this spectrum it also clears that there is no such peak was examine except the nanocomposite, which further indicates that the

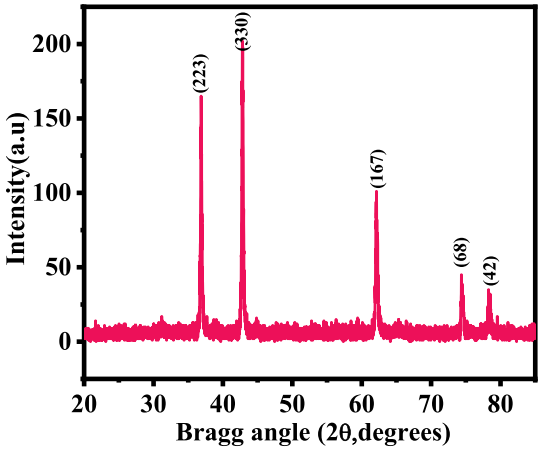

Fig. 1. X-ray diffraction of the prepared NiCoO nanocomposite.

prepared structures are pure material [46]. The particle size of the prepared composite was analyzed via the well-known scherrer equation as described earlier [47]. The parameters such as X-ray diffraction pattern phases, peaks, FWHM, crystallite size and average diameter was tabulated as below.

$$D = \frac{0.9\lambda}{\beta cos\theta}$$

S. N.	Phase	Peak	FWHM	Crystallite Size D (nm)	D nm (Average Size)
1.	223	36.87	0.26733	31.32489	26.98650
2.	330	42.82	0.28292	30.16175	
3.	167	62.13	0.35242	26.31717	
4.	68	74.45	0.38927	25.63050	
5.	42	78.37	0.47677	21.49791	

In this equation λ is the wavelength of X-ray radiation source, β is full-width at half-maximum in [FWHM] radians, θ is Bragg's diffraction angle. The calculation was measured with the help of X-ray diffraction software (Origin pro 8, 2018) with Gaussian lorentzian fitting Program. The average value of particle sizes is ~27 nm.

3.1.1. Structural evaluation of nanocomposite/prepared powder

The structural evaluation of the prepared nanocomposite in the form of black powder was analyzed via SEM and achieved data is represented as Fig. 2. The image (Fig. 2a and b) shows the lower magnification image of prepared NPs in a high density with larger areas are seen in the image. Several aggregated particles are seen in this image, where they are combined with each other and some are seems to be individual. At higher magnification, it signifies that the several NPs are seen in spherical in shape in aggregated form (Fig. 2c and d). From the observation the prepared NPs exhibit smooth surfaces, with full area of NPs. Further for more clarification of the morphological examination of the prepared powder sample was analyzed via TEM and the obtained result is presented as Fig. 3. The analysis shows at low magnified images, NPs are in a group with different sized particles (Fig. 3a). The TEM image depicts that synthesized product and the acquired data clearly reveals that the NPs are in spherical and ellipsoidal in shape. At high magnification, that the prepared nanostructures are in spherical shaped NPs with an average diameter are about 27–30 nm (Fig. 3b), which are full agreement with SEM and XRD observations (Figs. 1 and 2).

3.1.2. Functional characterization (FTIR spectroscopy) of nanocomposite

The functional characteristic of the prepared nanocomposite was examined via FTIR spectroscopy as stated in the experimental section, the analysis was evaluated with KBr in the ranges from 4000 to 400 cm^{-1}. Fig. 4 demonstrates a wide and superficial peak acquired in the range of 3200–3600 cm^{-1} indicates the stretched mode of molecular vibration for hydroxyl (O–H) group [48]. The small starched peak at 2300–2400 denotes the atmospheric CO_2. The intense peak at 1639 cm^{-1} shows the twist/bend mode of vibration in water (HOH) [48] molecule. The symmetric and asymmetric stretching modes of vibration for nitro group were also observed at 1381 and 885 cm^{-1}. The peaks at 667 cm^{-1} and 489 cm^{-1} denotes the formation of nickel cobalt composite (NiCoO). The functional change in the material states that the hydroxide molecules changes to metal oxides [46] (Fig. 4).

3.2. X-ray photoelectron spectroscopy (XPS)

To know the surface behavior of metallic nanocomposite (NiCoO), the sample was analyzed with X-ray photoelectron spectroscopy (XPS) and the obtained results are presented as Fig. 5. The acquired wide and narrow scan spectra of Ni, Co and oxygen are shown in Fig. 5a. Including these the carbon narrow scan spectra which is references at 284.38 eV was also check and presented. The narrow scan peaks of metals (Ni, Co, O and C) can be seen in all the spectrums (Fig. 5b to e). From the survey spectra, it reveals that only metal peaks binding energies such as C_{1s} at 284.38eV, O_{1s} at 530.08eV, Co_{2p} at 780.08eV and Ni_{2p} 855.08eV are observed in the spectrum, which denotes that the processed nanocomposite nanomaterial is highly pure without any additive or impurities [45,49]. From the survey graph it can be very claer and seen that the Na peak is not observed in the spectrum, which is due to complete washing of prepared compound, again confirm the purity of the processed material. Further analysis were carried and narrow scan spectra were analyzed for each element such as Co2p, Ni2p, O1s and C1s peaks.

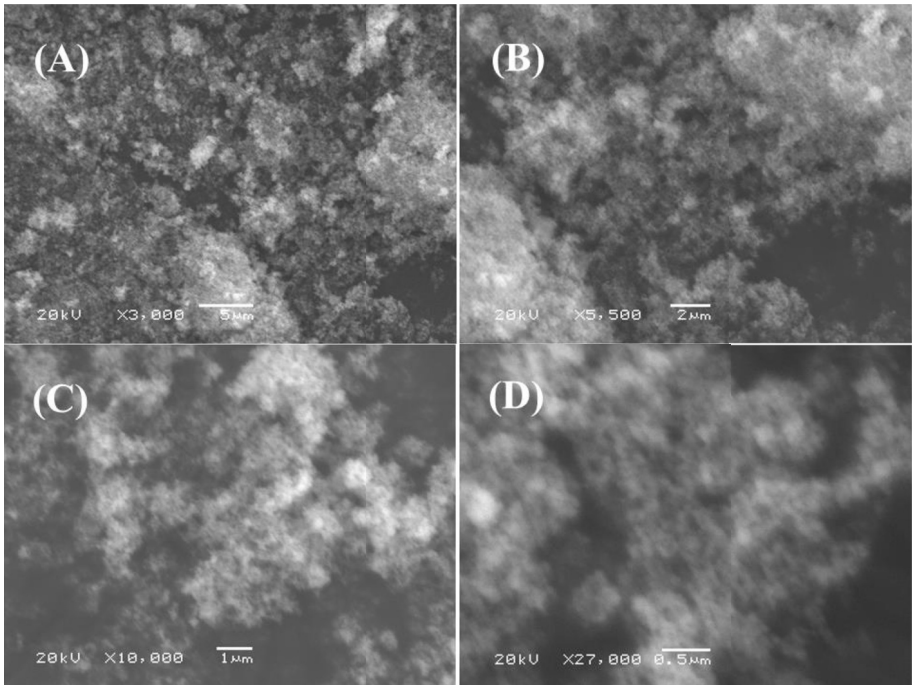

Fig. 2. SEM images of NiCoO nanocomposite: (a–b) captured at low magnification whereas (c and d) took at high magnified scale of NiCoO.

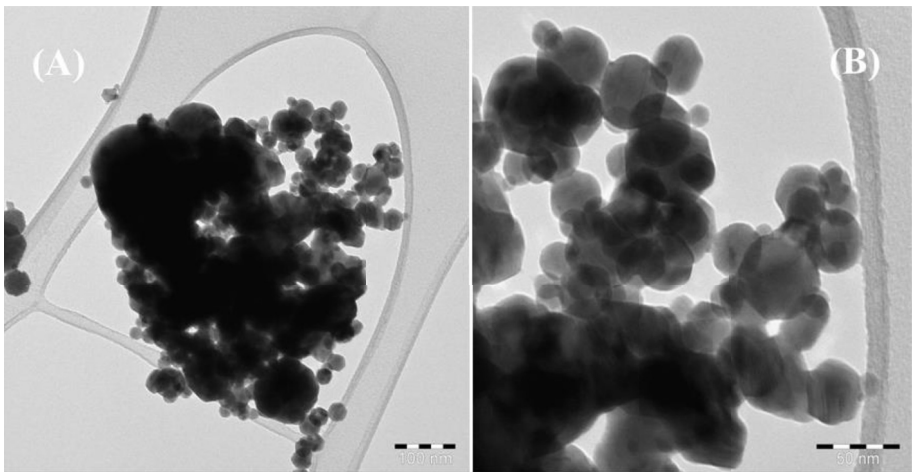

Fig. 3. Shows the TEM images at low (a) and high (b) magnification of prepared NiCoO.

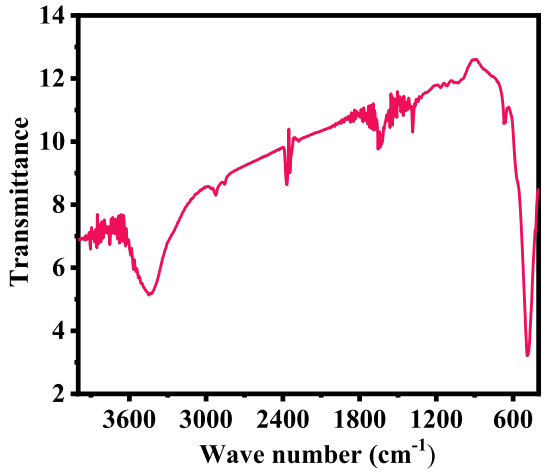

Fig. 4. FTIR spectrum shows the functional characteristic of grown NiCoO.

The acquired core level spectra of Ni2p was centered at 855.38 eV (Fig. 5b). The well-defined narrow scan spectra for Co_{2p} centered at 780.08eV (Fig. 5c) whereas O1s regions were centered at two regions 529.38 and 530.88 respectively, which corresponds to the surface hydroxyl (O–H) group and peak centered at 531.0 eV is attributed O^{2-} oxygen vacancies in the processed composite material (Fig. 5d) [45,49,50]. The references peak of carbon (C1s) at 284.38 eV, which may be due to atmospheric contamination or ambient acquaintance to the sample (Fig. 5e). The observation indicates that the nanocomposite (NiCoO) is highly pure material and it's consistent with also to XRD, SEM, FTIR and TEM analysis.

3.3. Electrochemical/cyclic voltammetry (CV) studies

Initially the formed electrode based on the prepared nanocomposite of NiCoO (area 2 × 2 cm^2) on NiCoO/GCE was checked in absence and presence of hydrazine (10 μL) in 100 mL of PBS (0.1 M, pH 7.2) solution with the scan rate of 100 mV/s. From the obtained spectra, it can be seen that good activity for hydrazine oxidation [2]. As can be seen from the spectra, the set potential and current (0.99 V, 11.65 × 10^{-4}) for hydrazine solution respectively [3] was moved to less value with and without hydrazine solution (0.98 V), and current was 9.35 × 10^{-4}, confirms that the prepared modified electrode based on NiCoO/GCE is much efficient for the transport of electron and oxidize the hydrazine [1] solution (Fig. 6).

3.4. Effect of hydrazine concentration on modified electrode (NiCoO/GCE)

To assess the routine investigation of current and potential (I-V) for the modified electrode NiCoO/GCE with dissimilar concentration (2, 4, 6, 8 and 10 μL) of hydrazine electrolyte in 100 mL PBS and the obtained result is presented as Fig. 7. The stock solution of hydrazine was prepared for the study of different concentration of hydrazine in PBS solution. To evaluate the routine investigation of current and potential (I-V) for the modified NiCoO/GCE with innumerable concentration of hydrazine in 100 mL PBS and presented as Fig. 7. The obtained spectrum represents at low range of hydrazine concentration solution, and this was examined at 100 mV with current and potential ranges from −1.0 to 1.0 V. As illustrated (Fig. 7), that current at anodic peak is directly consistent to the hydrazine concentration , rises with the rise of concentration of hydrazine solution. It assumed that when the current in the form of ions increases with the increase of hydrazine concentration which resembles to the fast electrons transfer at the conduction band. A high potential of anodic peak was also observed from another experiments, when hydrazine was used at high concentration level. The electron was displaced due to the increased amount of hydrogen ions in the solution (Fig. 7).

3.5. Effect of scan rates

For more detail to the scan rate and catalytic reactions between the hydrazine and modified NiCoO/ GCE electrode, which involved in the sensing process at different scan rates (10, 20, 50 and 100 mVs^{-1}) were evaluated and presented as Fig. 8. The scan rate exhibit that the peak currents increase on increasing the scan rate, in 0.1 M PBS solution, confirms that the oxidation process is diffusion controlled. For more detail associated to the scan rate and catalytic reactions between the hydrazine and NiCoO/GCE electrode, which involved in the sensing process at different scan rates (10, 20, 50 and 100 mVs^{-1}) were evaluated and presented as Fig. 8. A successive response at different scan rate of hydrazine of 0.1 M PBS solution of pH 7.2 was observed and presented as Fig. 8. The enhancement in current was observed after at various scan rates (10, 20, 50 and 100 mVs^{-1}). From the obtained graph and it can be concluded and show the relation between the current and potential enhancement of fabricated hydrazine sensor.

3.6. Effect of time response

To know the prepared sensor selectivity and reproducibility, the time response was also measured from 0 to 1200 s (Fig. 9). A sequential time response was observed at different time span for the prepared NiCoO/

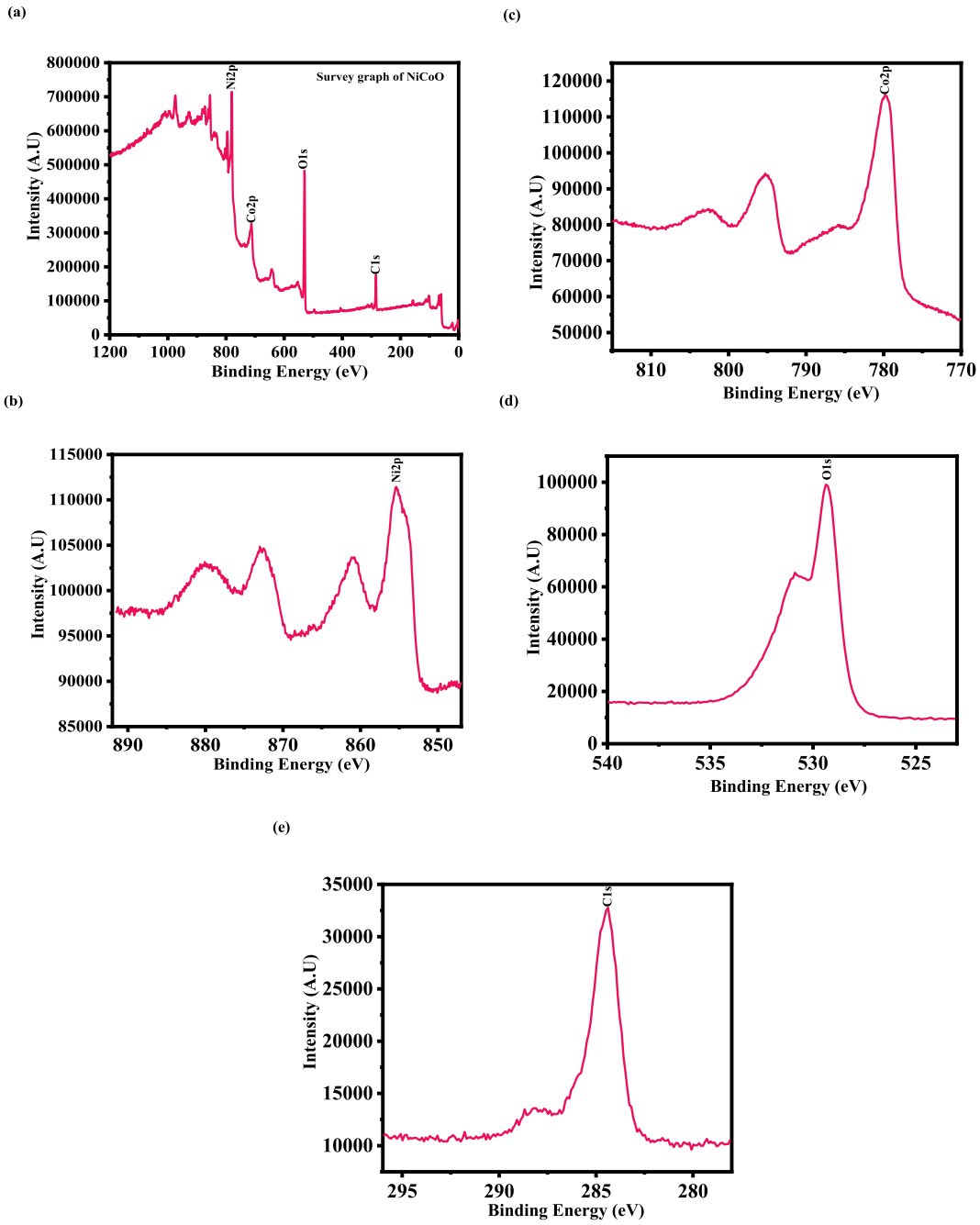

Fig. 5. X-ray photoelectron spectroscopy: (a) survey graph, (b) Ni 2p, (c) Co2p, (d) O1s and (e) shows the C1s spectra for the NiCoO nanocomposite samples.

GCE based hydrazine sensor. At 100s response was very minute (-11.84×10^{-4}) in the current but when the time span increases at 200s, 300s, 400s, 500s, 600s, 700s, 800s, 900s, 1000s, 1100s and 1200s current enhances to -5.920×10^{-4}, -3.82×10^{-4}, -2.72×10^{-4}, -2.11×10^{-4}, -1.76×10^{-4}, -1.50×10^{-4}, -1.34×10^{-4}, -1.21×10^{-4}, -1.10×10^{-4}, -1.03×10^{-4}, and -9.74×10^{-5} consequently for the prepared electrode. The obtained data states that the produced sensor is specific, selective, reproducible and exhibits enough sustainability for longer time [51].

3.7. Electrochemical impedance spectroscopy (EIS) studies

The EIS is a measurement technique to know the relation between the resistance and conductance for the prepared electrode (NiCoO/GCE) with varied concentration of electrolyte in frequency ranges from 0.01 Hz to 10 kHz and the result presented as Fig. 10. The X-axis which shows the 'Z' represents the ohmic and Y axis "-Z" represents the capacitive property in the Nyquist plot. Generally the impedance conquered from high to low frequency regions consequently. In the obtained result, the acquired semicircle curve of electrochemical impedance shows the smaller charge transfer resistance. The present work indicates that the wide semicircle is in high-frequency region was observed and analogous to the electron-transfer limited process. The inner diameter of semi-circle, represents the high frequency and resistance charge transfer ((Rct), which controls the electron transfer kinetics of the redox probe at electrode/electrolyte interface. As per the well-known fact that the larger semicircle curve illustrates a high interfacial Rct, which results from the poor electrical conductivity of the prepared/active materials. From the acquired results in the form of curve represent as Fig. 10, shows that diameter of semicircle at low hydrazine concentrations are

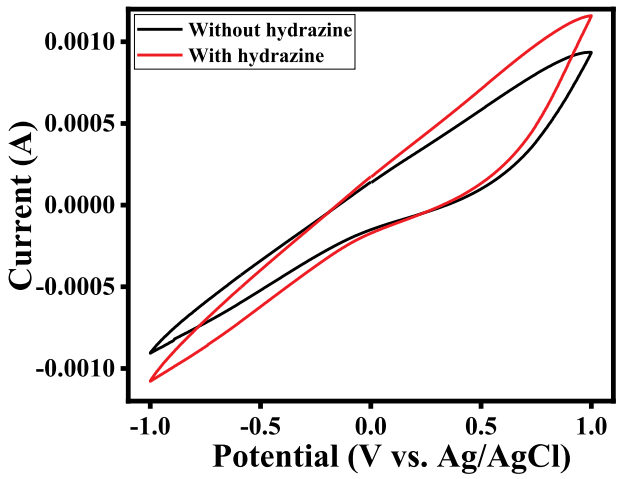

Fig. 6. Current and potential response of NiCoO supported nanocomposite/GCE in absence and presence of hydrazine at scan rate of 100 mV/s.

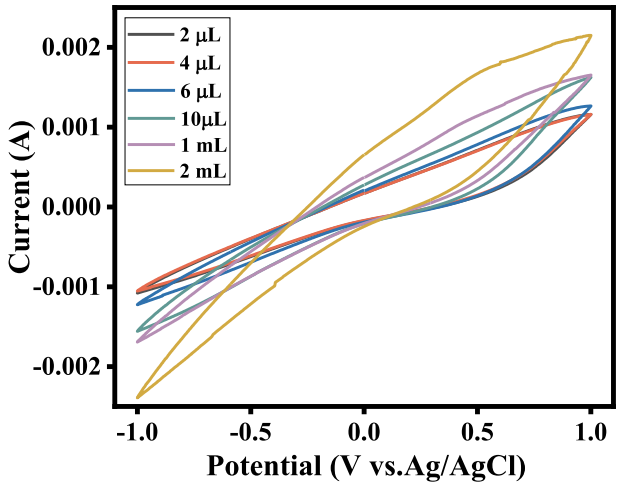

Fig. 7. Current and potential response of NiCoO/GCE at low range concentrations (from 2 µL to 10 µL) of hydrazine into 0.1 M PBS solution (pH 7.2). The scan rate is 100 mV/s.

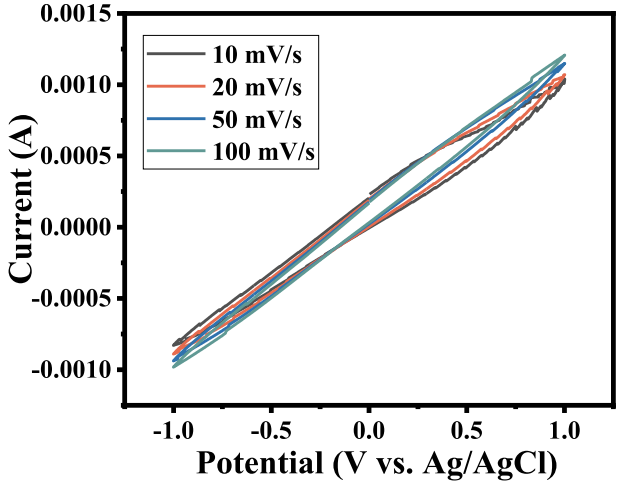

Fig. 8. CV obtained for NiCoO/GCE at in 0.1 M PBS containing hydrazine solutions at various scan rates 10, 20, 50, 100 mVs^{-1}.

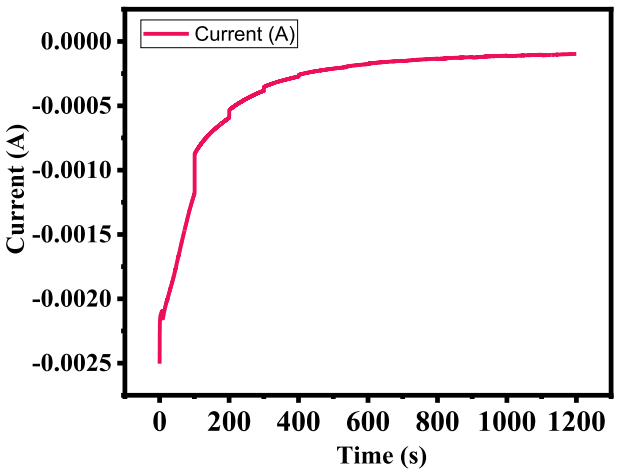

Fig. 9. Amperometric response of NiCoO/GCE with successive addition of hydrazine into 0.1 M PBS buffer solution (pH 7.0), which depicts the time (0–1200 s) and current spectra for the reliability and reproducibility of the optimized data.

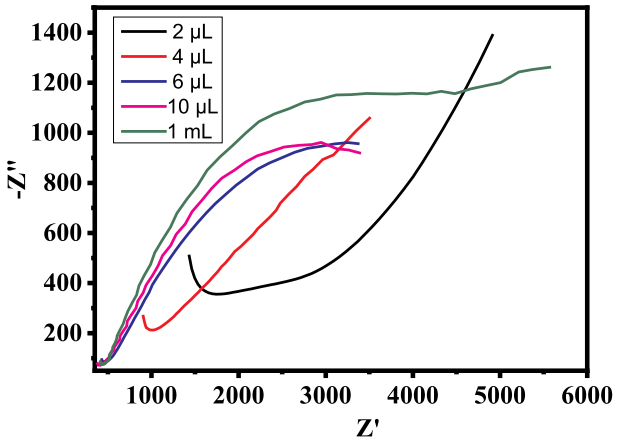

Fig. 10. Electrochemical impedance spectra of NiCoO/GCE modified GCE towards various high concentrations (from 1 to 5 mL) of hydrazine into 0.1 M PBS solution (pH7).

larger as associated to the higher concentrations, which may be due to high Rct values in the NiCoO composite electrode [52]. This is may be due to the nickel and cobalt itself exhibit high catalytic properties.

3.8. Possible mechanism and discussion

The composites are the materials which exhibit high band gap due to the mixing of other material, which enhances the electroactive property of the material. In present work, the bimetallic oxide (NiCoO) nanostructures were formed via solution process with the use of nitrate salt of nickel and cobalt at very low refluxing temperature. The formed nanostructures were well characterized with XRD, SEM, TEM and FTIR spectroscopy and applied as an electrode material. In this experiment, we have opted a long range of hydrazine for the electrochemical detection from low to high concentration (2 µL–2 mL/100 mL PBS), which works as an electrolyte in solution. The prepared working electrode NiCoO/GCE plays an important role in electron transportation. The nanocomposite based (NiCoO/GCE) electrode can be utilized for the large scale industrial and environmental samples detection of hydrazine. The basic principle for the developed NiCoO/GCE electrode works on the varied concentration of analyte (hydrazine) and their adsorption and conductance on NiCoO/GCE electrode. When the processed material

was pasted on GCE and insurted in the solution of analyte (hydrazine)in PBS. The atmospheric oxygen, which has an ability to physisorption of electrode (NiCoO/GCE) and have possibility to interchange from various spots and ionized (O^{-}_{ads}) through the elimination of electron from the conduction band then convert into their oxidized from (O^{-} or O^{2-}) on surface layer of NiCoO, form a charge layer between surface layer of NPs and analyte [53,54]. This surface adsorbed oxygen amplifies the potential of the prepared electrode and improved the resistance. This development leads a reduction in conductance and increase in potential of the formed (NiCoO/GEC) electrode. From this experiment it's hypothesized that at a crucial change in the concentration (low to high) of analyte provides higher efficiency and greater resistivity. The sensor result influences on the basis of used nanostructured material in their different symmetrical organization, chemical properties, mode of preparation etc. The NPs which exhibit enhanced surface area and doping with other NPs increases the band gap of material, which exhibit high electron transportation passages and also facilitates higher sensing aptitude as compared to others nanostructures. The doping which is a powerful tool to modify the nanostructural physical and chemical characteristic such as optical, electrochemical, sensing properties etc, provides extended interface for various types of sensing devices. The semiconductor metal oxides nanostructures, which have a tendency to produce a fruitful environment on their surfaces and allows to access the role of analyte via adsorption process. The enhanced sensitivity, stability of the material and improved reproducible properties validated the higher rate of electron transportation between the NiCoO/GEC and analyte (hydrazine molecule). The immobilization of the nanostructures and feasibility with analyte affects the reaction/response time and their enactment of the produced sensor and improved with the utilization of proper catalyst which spill over the entire surface of the NiCoO/GEC electrode. The used catalyst play a significant character to accelerate the reaction with initially adsorbed surface oxygen of the material, also upsurge the conductance and response of the formed electrode [55,56].

4. Conclusions

The conclusion of the present work states that the nanocomposite of NiCoO was formed via solution process with the use of nickel nitrate hexahydrate ($Ni(NO_3)_2{\cdot}6H_2O$), cobalt nitrate hexahydrate ($Co(NO_3)_2{\cdot}6H_2O$) and NaOH in a very less time (60 min) span. The processed nanocomposite material was also well characterized in relation to their morphological, chemical and electrochemical studies. Initially the material was characterized in terms of their structural and chemical properties via the XRD, to examine the crystalline properties whereas the morphology of NPs were accessed through SEM and it reveals that the individual particles size is in the range of about 27–30 nm with spherical in shape. The morphology was again confirmed with the use of TEM and it justifies the SEM observations. The functional properties were also examined via FTIR spectroscopy. Including this, the elemental study was also conducted to know the core level binding energies of Ni2p, Co2p, O1s, C1s with detailed survey. The nanocomposite was applied as an efficient nanosensor against the catalyst N_2H_4 chemical sensor. The CV was applied to know the ionic exchange in a liquid medium at very low concentration (2 μL N_2H_4/100 mL PBS) with hydrazine solution were observed. A sequential change in the oxidation and reduction peaks were examined which indicates that the obtained sensor is specific and can be useful for the large scale detection. The obtained sensors selectivity and reproducibility were also observed from zero to 1200s deals that the sensors exhibit enough sustainability for longer period.

Declaration of competing interest

The authors declare that there are no conflicts of interest.

Acknowledgement

The authors extend their appreciation to the Deanship of Scientific Research at King Saud University for funding this work through research group no. RG-218.

References

[1] M. Vogel, A. Büldt, U. Karst, Hydrazine reagents as derivatizing agents in environm ental analysis– a critical review, J. Anal. Chem. 366 (2000) 781–791.
[2] D.P. Elder, D. Snodin, A. Teasdale, Control and analysis of hydrazine, hydrazides and hydrazones-genotoxic impurities in active pharmaceutical ingredients (APIs) and drug products, J. Pharm. Biomed. Anal. 54 (2011) 900–910.
[3] W.X. Yin, Z.P. Li, J.K. Zhu, H.Y. Qi, Effects of NaOH addition on performance of the direct hydrazine fuel cell, J. Power Sources 182 (2008) 520–523.
[4] S. Amlathe, V.K. Gupta, Spectrophotometric determination of trace amounts of hydra- zine in polluted water, Analyst 113 (1988) 1481–1483.
[5] S. Garrod, M.E. Bollard, A.W. Nicholls, S.C. Connor, J. Connelly, J.K. Nicholson, E. Holmes, Integrated metabonomic analysis of the multiorgan effects of hydrazine toxicity in the rat, Chem. Res. Toxicol. 18 (2005) 115.
[6] G. Choudhary, H. Hansen, Human health perspective of environmental exposure to hydrazines: a review, Chemosphere 37 (1998) 801–843.
[7] E.H. Vernot, J.D. MacEwen, R.H. Bruner, C.C. Haus, E.R. Kinkead, Long-term inhalation toxicity of hydrazine, Fundam. Appl. Toxicol. 5 (1985) 1050–1064.
[8] World Health Organization, Environmental Health Criteria 68: Hydrazine, Geneva, Switzerland, 1987, pp. 1–89.
[9] M.H. Jazayeri, T. Aghaie, A. Avan, A. Vatankhah, M.R.S. Ghaffari, Colorimetric detection based on gold nanoparticles (GNPs): an easy, fast, inexpensive, low-cost and short time method in detection of analytes (protein, DNA, and ion), Sens. Bio-Sens. Res. 20 (2018) 1–8.
[10] M. Sun, L. Bai, D.Q. Liu, A generic approach for the determination of trace hydrazine in drug substances using in situ derivatization-headspace GC-MS, J. Pharm. Biomed. Anal. 49 (2009) 529–533.
[11] C.M. Morenoa, T. Stadler, A.A. Silva, L.C.A. Barbosa, M.E.L.R. Queiroz, Determination of maleic hydrazide residues in garlic bulbs by HPLC, Talanta 89 (2012) 369–376.
[12] G.E. Collins, Gas-phase chemical sensing using electrochemiluminescence, Sens. Actuators B B35 (1996) 202–206.
[13] S. Ikeda, H. Satake, Y. Kohri, Flow Injection Analysis with Amperometric Detector utilizing the redox reaction of iodate ions, Chem. Lett. 13 (1984) 873–876.
[14] C. Gojon, B. Dureault, N. Hovnanian, C. Guizard, A comparison of immobilization sol-gel methods for an optical chemical hydrazine sensor, Sens. Actuators B 38 (1–3) (1997) 154–162.
[15] M.A. Koupparis, T.P. Hadjiioannou, Indirect potentiometric determination of hydra zine, isoniazid, sulphide and thiosulphate with a chloramine-T ion-selective electrode, Talanta 25 (8) (1978) 477–480.
[16] L. Zheng, J.F. Song, Curcumin multi-wall carbon nanotubes modified glassy carbon electrode and its electrocatalytic activity towards oxidation of hydrazine, Sens. Actuators, B 135 (2009) 650–655.
[17] V. Singh, D. Joung, L. Zhai, S. Das, S.I. Khondaker, S. Seal, Graphene based materials: past, present and future, Prog. Mater. Sci. 56 (8) (2011) 1178–1271.
[18] D.R. Dreyer, S. Park, C.W. Bielawski, R.S. Ruoff, The chemistry of graphene oxide, Chem. Soc. Rev. 39 (2010) 228–240.
[19] C. Wang, L. Zhang, Z. Guo, J. Xu, H. Wang, K. Zhai, X. Zhuo, A novel hydrazine electrochemical sensor based on the high specific surface area graphene, Microchim Acta169 (2010) 1–6.
[20] S.H. Wu, F.H. Nie, Q.Z. Chen, J.J. Sun, Electrocatalytic oxidation and nanomolar detection of hydrazine by luteolin electrodeposited at a multi-walled carbon nanotube and ionic liquid composite modified screen printed carbon electrode, Anal. Methods 2 (2010) 1729–1736.
[21] M.M. Ardakani, Z. Taleat, H. Beitollahia, H. Naeimi, Nanomolar concentrations determination of hydrazine by a modified carbon paste electrode incorporating TiO_2 nano particles, Nanoscale 3 (2011) 1683–1689.
[22] Y. He, J. Zheng, S. Dong, Ultrasonic-electrodeposition of hierarchical flower-like cobalt on petalage-like graphene hybrid microstructures for hydrazine sensing, Analyst 137 (2012) 4841–4848.
[23] B. Wu, Y. Kuang, X. Zhang, J. Chen, Noble metal nanoparticles/carbon nanotubes nanohybrids: synthesis and applications, Nano Today 6 (2011) 75–90.
[24] R. Muszynski, B. Seger, P.V. Kamat, Decorating graphene sheets with gold nano particles, J. Phys. Chem. C112 (2008) 5263–5266.
[25] A.A. Lazarides, K.L. Kelly, T.R. Jensen, G.C. Schatz, Optical properties of metal nanoparticles and nanoparticle aggregates important in biosensors, J. Mol. Struct.: THEOCHEM 529 (2000) 59–63.
[26] C.N.R. Rao, G.U. Kulkarni, P.J. Thomas, P.P. Edwards, Metal nanoparticles and their assemblies, Chem. Soc. Rev. 29 (2000) 27–35.
[27] C. Wang, C. Yu, Detection of chemical pollutants in water using gold nanoparticles as sensors: a review, Rev. Anal. Chem. 32 (2013) 1–14.
[28] P.V. Dudin, P.R. Unwin, J.V. Macpherson, Electro-oxidation of hydrazine at gold nano particle functionalised single walled carbon nanotube network ultra microelectrodes, Phys. Chem. Chem. Phys. 13 (2011) 17146–17152.
[29] Q. Wan, Y. Liu, Z. Wang, W. Wei, B. Li, J. Zou, N. Yang, Graphene nanoplatelets supported metal nanoparticles for electrochemical oxidation of hydrazine, Electrochem. Commun. 29 (2013) 29–32.

[30] G. Hua, Z. Zhou, Y. Guo, H. Hou, S. Shao, Electrospun rhodium nanoparticle-loaded carbon nanofibers for highly selective amperometric sensing of hydrazine, Electrochem. Commun. 12 (2010) 422–426.
[31] R. Ahmad, N. Tripathy, D.U.J. Jung, Y.B. Hahn, Highly sensitive hydrazine chemical sensor based on ZnO nanorods field-effect transistor, Chem. Commun. 50 (2014) 1890–1893.
[32] F.A. Harraz, A.A. Ismail, S.A. Al-Sayari, A. Al-Hajry, M.S. Al-Assiri, Highly sensitive amperometric hydrazine sensor based on novel a-Fe_2O_3/crosslinked polyaniline nanocomposite modified glassy carbon electrode, Sens. Actuators B Chem. 234 (2016) 573–582.
[33] S.P. Kim, H.C. Choi, Reusable hydrazine amperometric sensor based on Nafion-coated TiO_2-carbon nanotube modified electrode, Sens. Actuators B Chem. 207 (2015) 424–429.
[34] Y. He, W. Huang, Y. Liang, H. Yu, A low-cost and label-free assay for hydrazine using MnO_2 nanosheets as colorimetric probes, Sens. Actuators B Chem. 220 (2015) 927–931.
[35] D. Han, X. Jing, J. Wang, P. Yang, P.D. Song, J. Liu, Porous lanthanum doped NiO microspheres for supercapacitor application, J. Electroanal. Chem. 682 (2012) 37–44.
[36] V.S. Manikandan, B.R. Adhikari, A. Chen, Nanomaterial based electrochemical sensors for the safety and quality control of food and beverages, Analyst 143 (2018) 4537–4554.
[37] G. Hu, C. Tang, C. Li, H. Li, Y. Wang, H. Gong, The sol-gel-derived nickel-cobalt oxides with high supercapacitor performances, J. Electrochem. Soc. 158 (2011) A695–A699.
[38] S.M. Gates, J.N. Russell, J.T. Yates, Bond activation sequence observed in the chemisorption and surface reaction of ethanol on Ni(111), Surf. Sci. 171 (1986) 111–134.
[39] M.A.A. Rahim, R. Abdel Hameed, M. Khalil, Nickel as a catalyst for the electro-oxidation of methanol in alkaline medium, J. Power Sources 134 (2004) 160–169.
[40] C. Fan, D. Piron, A. Sleb, P. Paradis, Study of electrodeposited nickel-molybdenum, nickel-tungsten, cobalt-molybdenum, and cobalt-tungsten as hydrogen electrodes in alkaline water electrolysis, J. Electrochem. Soc. 141 (1994) 382–387.
[41] I.A. Raj, K. Vasu, Transition metal-based hydrogen electrodes in alkaline solution — electrocatalysis on nickel based binary alloy coatings, J. Appl. Electrochem. 20 (1990) 32–38.
[42] X. Sun, F. Li, J. Shi, Y. Zheng, H. Su, L. Sun, S. Peng, C. Qi, Gold nanoparticles supported on MgOx-Al_2O_3 composite oxide: an efficient catalyst for selective hydrogenation of acetylene, Appl. Surf. Sci. 487 (2019) 625–633.
[43] L. Liu, Y. Zhao, P. Song, Z. Yang, Q. Wang, Ppb level triethylamine detection of yolk- shell SnO_2/Au/Fe_2O_3 nanoboxes at low-temperature, Appl. Surf. Sci. 476 (2019) 391–401.
[44] Q. Li, S. Zheng, J. Pu, W. Wang, L. Li, L. Wang, Revealing the failure mechanism and designing protection approach for MoS_2 in humid environment by first-principles investigation, Appl. Surf. Sci. 487 (2019) 1121–1130.
[45] Y. Wen, S. Peng, Z. Wang, J. Hao, T. Qin, S. Lu, J. Zhang, D. He, X. Fan, G. Cao, Facile synthesis of ultrathin NiCo2S4 nano-petals inspired by blooming buds for high- performance supercapacitors, J. Mater. Chem. A 5 (2017) 7144–7152.
[46] D. Devadatha, R. Raveendran, Structural and dielectric characterization of nickel-cobalt oxide nanocomposite, J. Mater. Sci. Eng. S11 (2013) 003, https://doi.org/10.4172/2169-0022.S11-003.
[47] B.D. Cullity, Elements of X-Ray Diffraction, Addison-Wesley Publishing Company, Reading, MA, 1978.
[48] S.G. Ansari, R. Wahab, Z.A. Ansari, Y.S. Kim, G. Khang, A. Al-Hajry, H.S. Shin, Effect of nanostructure on the urea sensing properties of sol–gel synthesized ZnO, Sens. Actuators B 137 (2009) 566–573.
[49] X. Hana, X. Wu, C. Zhong, Y. Deng, N. Zhao, W. Hua, NiCo2S4 nanocrystals anchored on nitrogen-doped carbon nanotubes as a highly efficient bifunctional electrocatalyst for rechargeable zinc-air batteries, Nano Energy 31 (2017) 541–550.
[50] Y. Xiao, P. Zhang, X. Zhang, X. Dai, Y. Ma, Y. Wang, Y. Jiang, M. Liu, Y. Wang, Bimetallic thin film NiCo–NiCoO2@NC as a superior bifunctional electrocatalyst for overall water splitting in alkaline media, J. Mater. Chem. A 5 (2017) 15901–15912.
[51] R. Wahab, N. Ahmad, M. Alam, A.A. Ansari, Nanocubic magnesium oxide: towards hydrazine sensing, Vacuum 155 (2018) 682–688.
[52] R. Gopalakrishnan, Y. Li, J. Smekens, A. Barhoum, G.V. Assche, N. Omar, J. V. Mierlo, Electrochemical impedance spectroscopy characterization and parameterization of lithium nickel manganese cobalt oxide pouch cells: dependency analysis of temperature and state of charge, Ionics 25 (1) (2019) 111–123.
[53] S. Chaudhary, A. Umar, K.K. Bhasin, S. Baskoutas, Chemical sensing applications of ZnO nanomaterials, Materials 11 (2018) 287, https://doi.org/10.3390/ma11020287.
[54] M.M. Rahman, M.M. Alam, A.M. Asiri, Selective hydrazine sensor fabrication with facile low-dimensional Fe_2O_3/CeO_2 nanocubes, New J. Chem. 42 (2018) 10263–10270.
[55] A. Umar, M.S. Akhtar, A. Al-Hajry, M.S. Al-Assiri, G.N. Dar, M.S. Islam, Enhanced photocatalytic degradation of harmful dye and phenyl hydrazine chemical sensing using ZnO nano-urchins, Chem. Eng. J. 262 (2015) 588–596.
[56] S.K. Mehta, Khushboo, A. Umar, Highly sensitive hydrazine chemical sensor based on mono-dispersed rapidly synthesized PEG-coated ZnS nanoparticles, Talanta 85 (2011) 2411–2416.